Applied Physics Letters

RESEARCH ARTICLE | JULY 08 2025

Valley polarization and anomalous valley Hall effect in altermagnet Ti_2Se_2S with multipiezo properties

Xin Hu; Weihang Zhao; Wenjun Xia; Hanbo Sun; Chao Wu; Yin-Zhong Wu ; Ping Li

Appl. Phys. Lett. 127, 011905 (2025)
https://doi.org/10.1063/5.0278751

Applied Physics Letters ARTICLE pubs.aip.org/aip/apl

Valley polarization and anomalous valley Hall effect in altermagnet Ti_2Se_2S with multipiezo properties

Cite as: Appl. Phys. Lett. **127**, 011905 (2025); doi: 10.1063/5.0278751
Submitted: 2 May 2025 · Accepted: 22 June 2025 ·
Published Online: 8 July 2025

Xin Hu,[1] Weihang Zhao,[1] Wenjun Xia,[1] Hanbo Sun,[1] Chao Wu,[1] Yin-Zhong Wu,[2,a)] and Ping Li[1,3,4,a)]

AFFILIATIONS

[1]State Key Laboratory for Mechanical Behavior of Materials, Center for Spintronics and Quantum System, School of Materials Science and Engineering, Xi'an Jiaotong University, Xi'an, Shaanxi 710049, China
[2]School of Physical Science and Technology, Suzhou University of Science and Technology, Suzhou 215009, China
[3]State Key Laboratory of Silicon and Advanced Semiconductor Materials, Zhejiang University, Hangzhou, 310027, China
[4]State Key Laboratory for Surface Physics and Department of Physics, Fudan University, Shanghai 200433, China

[a)]**Authors to whom correspondence should be addressed:** yzwu@usts.edu.cn and pli@xjtu.edu.cn

ABSTRACT

Recently, altermagnets demonstrate numerous unique physical phenomena due to their inherent antiferromagnetic coupling and spontaneous spin splitting, which are anticipated to enable innovative spintronic devices. However, the rare two-dimensional altermagnets have been reported, making it difficult to meet the requirements for high-performance spintronic devices on account of the growth big data. Here, we predict a stable monolayer Ti_2Se_2S with out-of-plane altermagnetic ground state and giant valley splitting. The electronic properties of altermagnet Ti_2Se_2S are highly dependent on the onsite electron correlation. Through symmetry analysis, we find that the valleys of X and Y points are protected by the mirror M_{xy} symmetry rather than the time-reversal symmetry. Therefore, the multipiezo effect, including piezo-valley and piezomagnetism, can be induced by the uniaxial strain. The total valley splitting of monolayer Ti_2Se_2S can be as high as ~500 meV. More interestingly, the direction of valley polarization can be effectively tuned by the uniaxial strain; based on this, we have defined logical 0, +1, and −1 states for data transmission and storage. In addition, we have designed a schematic diagram for observing the anomalous Hall effect in the experiment. Our findings have enriched the candidate materials of two-dimensional altermagnet for the ultrafast and low power consumption device applications.

Altermagnetism, a recently discovered magnetic phase, brought about widespread attention due to the spin splitting and zero net magnetization.[1–4] Importantly, the emergence of these unique phenomena does not require the spin–orbit coupling (SOC) effect.[1,2] In addition, the spin-dependent Fermi surface in altermagnets exhibit the planar or bulk *d*-wave, *g*-wave, or *i*-wave symmetry in momentum space.[1,2] It indicates that the altermagnet has the virtues of resisting external field perturbations, switching speed, ultrafast spin dynamics of antiferromagnet (AFM), and intrinsic ferromagnetic spin splitting. These features of altermagnetic materials can induce a series of unique quantum phenomena, such as the spin splitting induced spin current generation;[5–7] the large anomalous Hall effect comparable to that of FM;[8] the significant spin Seebeck, crystal Nernst, and crystal thermal Hall effects;[9,10] the staggered spin-momentum interaction caused by the time-reversal symmetry breaking;[11] the tunneling and giant magnetoresistance effect;[12] the crystal chirality magneto-optical response;[13] the nonlinear transport;[14] the theoretically proposed spin-splitter torque[15] and experimentally confirmed;[16,17] and the nontrivial superconductivity;[18,19] which means broad application prospects. To date, the experimental investigation mainly focuses on three-dimensional materials such as MnTe,[4,20,21] RuO_2,[8,17] CrSb,[22–24] and Cr-doped $FeSb_2$.[25] When quantum is confined to a two-dimensional (2D) system, more abundant physical phenomena will emerge.[26,27] Unfortunately, there are a few 2D altermagnets suitable for experimental research, which is an urgent need to find more altermagnets.

Valley represents the third independent quantum degree of freedom for electrons, existing alongside charge and spin properties, which has caused extensive concern since it offers exceptional potential for realizing future devices featuring THz-speed operation, unprecedented capacity, ultra-low power consumption, and nonvolatile data

retention.[28–30] The valley index corresponds to the local energy extremal points in the band structure. To utilize the valley index as an information encoding parameter, controlled manipulation of valley carriers is essential to achieve valley polarization and to realize the anomalous valley Hall effect. Currently, there are two methods to achieve spontaneous valley polarization. One method is to break inversion symmetry (P) through ferroelectricity,[30] while the other is to break time-reversal symmetry (T) by magnetism.[31–36] They are named ferroelectric ferrovalley and magnetic ferrovalley. However, the altermagnets also break the T symmetry, how does it realize valley polarization?

In this work, based on the first-principles calculations, we predict that the 2D altermagnet Ti_2Se_2S is a candidate material with promising application prospects in multipiezo and valleytronic. Monolayer Ti_2Se_2S exhibits stable out-of-plane altermagnet properties. It shows the characteristics of semiconductor with the bandgap located at the X and Y points. Interestingly, the valence band maximum (VBM) and conduction band minimum (CBM) at the X point are spin down and spin up bands, respectively, while it is just the opposite at the Y point. Moreover, the transformation from metal to semiconductor is demonstrated with the increase in the Hubbard U value. Our results demonstrate that the uniaxial strain can effectively tune the magnitude and direction of valley polarization. In addition, the abundant multipiezo effect, including the piezoelectric and piezomagnetism, can be realized in monolayer Ti_2Se_2S. Based on these, we designed the devices of the anomalous valley Hall effect and the piezoelectric effect. The unique combination of physical properties in monolayer Ti_2Se_2S makes it a highly promising candidate material for multifunctional valleytronic and spintronic device applications.

Within the framework of density functional theory (DFT), we systematically explored the magnetic and electronic properties through the Vienna *ab initio* Simulation Package (VASP).[37–39] The exchange-correlation energy was treated within the Perdew-Burke-Ernzerhof (PBE) of the generalized gradient approximation (GGA).[40] The $21 \times 21 \times 1$ Γ-centered k meshes of Brillouin zone (BZ) are adopted. The plane wave basis set with a kinetic energy cutoff of 500 eV is employed. The structural optimizations are performed with a convergence criterion of 10^{-6} eV for total energy and −0.01 eV/Å for Hellmann-Feynman forces. A 20 Å vacuum layer is perpendicularly added to the 2D plane (c-axis direction) in the slab geometry, effectively suppressing spurious interactions between the monolayer and its periodic replicas. To describe strongly correlated 3d electrons of Ti,[41] the GGA + U method is used with the Coulomb repulsion U value of 3.0–4.0 eV. To investigate the dynamical stability, the phonon spectra are calculated using the PHONOPY package with a $3 \times 3 \times 1$ supercell.

Monolayer Ti_2Se_2S behaves a 2D square lattice with the point group of D_{4h} and the space group of P4/mmm, as shown in Fig. 1(a). The crystal structure consists of three atomic layers, which the Ti-S atomic plane is sandwiched between two Se atomic planes, similar to the monolayer V_2Se_2O.[6,42] The yellow dotted square indicates the unit cell. It shows a M_{xy} mirror and C_4 rotational symmetries, which is an important condition required for altermagnet. The Ti atom bonds with the surrounding four Se atoms and two S atoms, forming an octahedral crystal field. The lattice constant of monolayer Ti_2Se_2S is 4.53 Å, while the bond length of Ti-S and Ti-Se is 2.26 and 2.79 Å, respectively. As shown in Fig. 1(c), it exhibits the first Brillouin zone (BZ) including

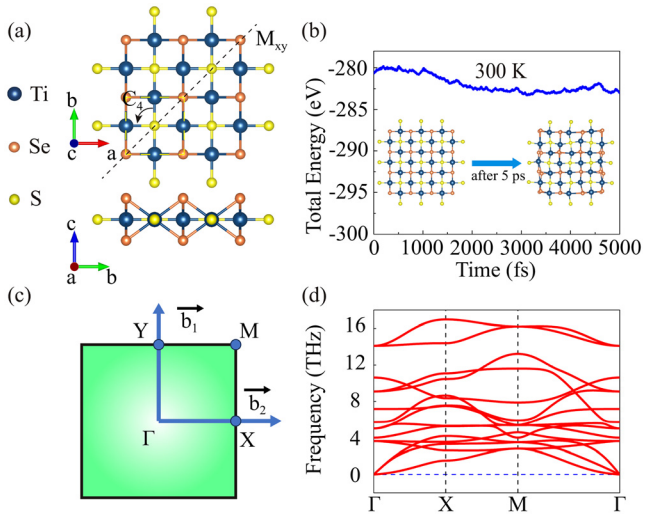

FIG. 1. (a) The top and side views of monolayer Ti_2Se_2S structure. The yellow dotted square denotes the unit cell. The cyan, orange, and yellow balls represent Ti, Se, and S elements, respectively. (b) The total energy fluctuation of monolayer Ti_2Se_2S during 5 ps AIMD simulation at 300 K. The final structures after AIMD simulation are exhibited in the insets. (c) The BZ of the square lattice is characterized by its reciprocal lattice vectors $\vec{b}_1$ and $\vec{b}_2$. The Γ, X, Y, and M are high-symmetry points in the BZ. (d) The phonon dispersion curves were calculated along the high-symmetry lines of the BZ.

the high-symmetry points. It is worth noting that the bond angle of Ti-S-Ti is exactly 180°, indicating a favorable AFM coupling according to the Goodenough-Kanamori-Anderson rule.[43–45] We evaluated the stability of monolayer Ti_2Se_2S from two aspects. On the one hand, we estimated its thermodynamic stability by *ab initio* molecular dynamics (AIMD). As shown in Fig. 1(b), the total energy of monolayer Ti_2Se_2S shows minimal fluctuation during 5 ps at 300 K, demonstrating its excellent thermal stability. On the other hand, we calculated the phonon spectrum to evaluate the dynamic stability. Figure 1(d) shows the absence of imaginary frequencies, indicating that the monolayer Ti_2Se_2S is dynamically stable.

To confirm the magnetic ground state of monolayer Ti_2Se_2S, we considered two typical magnetic configurations, namely, the AFM and ferromagnetic (FM) states. The calculation results show that the total energy of the AFM state is 66.53 meV lower than that of the FM state, indicating that the AFM is the magnetic ground state. Figure 2(a) shows its magnetic ground state configuration structure. The important factor for the stable existence of 2D magnetic materials is the presence of out-of-plane magnetic anisotropy energy (MAE). The out-of-plane MAE can effectively suppress the magnetic moment fluctuations caused by thermal disturbances and maintain the long-range magnetic order. The MAE is primarily derived from SOC interactions.[46] The MAE is defined as $MAE = E_{100} - E_{001}$, where E_{100} and E_{001} denote the total energy of the Ti atoms magnetic moment along [100] and [001] directions, respectively. The MAE of monolayer Ti_2Se_2S is 0.77 meV, which indicates that the direction of easy magnetization is along the out-of-plane. In addition, for the octahedral symmetry of monolayer Ti_2Se_2S, the MAE can be written in the form of angle dependence,

$$MAE = K_1 \cos^2\theta + K_2 \cos^4\theta, \quad (1)$$

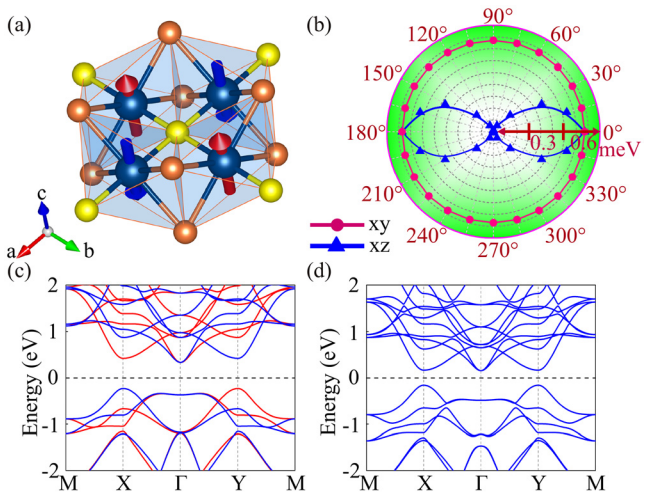

FIG. 2. (a) The magnetic configuration of monolayer Ti_2Se_2S and the octahedral crystal field. (b) The angular variation of MAE in monolayer Ti_2Se_2S, when the magnetization orientation is confined within the xz plane. (c) Spin-polarized band structure of monolayer Ti_2Se_2S. The red and blue lines denote spin up and spin down bands, respectively. (d) Band structure of monolayer Ti_2Se_2S with the SOC effect.

where K_1, K_2, and θ are the anisotropy constants and azimuthal angle of rotation, respectively. If $K_1 < 0$, it indicates that the easy magnetization direction is along the out-of-plane (z-axis), while $K_1 > 0$ suggests that it is beneficial to be parallel in the in-plane (x-axis). The MAE of monolayer Ti_2Se_2S shows a good fit of Eq. (1) as presented in Fig. 2(b), and it suggests a pronounced dependence of the MAE on the magnetization orientation within the xz plane. Moreover, the MAE maintains a value of 0.77 meV in the xy plane, which indicates the typical isotropic characteristic.

For the traditional AFM system with the combined T and P symmetry (PT), which connects the energy eigenvalues $E_\uparrow(\mathbf{k})$ and $E_\downarrow(\mathbf{k})$, ensuring the spin degeneracy, the P operation only converses the vector k. Therefore, it can be ensured that the eigenvalues are satisfied $PE_\uparrow(k) = E_\uparrow(-k)$. However, the T operation can reverse not only k but also spin, leading to the $TE_\uparrow(k) = E_\downarrow(-k)$. It indicates that the PT symmetry makes certain $E_\uparrow(k) = PTE_\uparrow(k) = E_\downarrow(k)$. The result presented is spin degenerate bands for the two opposite components. In addition, the translation operation (t) also produces $tE_\uparrow(k) = E_\uparrow(k)$. Therefore, the energy eigenvalue of traditional AFM system satisfies $PTtE_\uparrow(k) = E_\uparrow(k)$. Noted that the spin and real spaces are completely decoupled in the ignoring SOC effect. Consequently, the spin reversal operation U generates $UE_\uparrow(k) = E_\uparrow(k)$, where U is exclusively defined for collinear spin configurations.[47–49]

Through the aforementioned analysis, the spin splitting of monolayer altermagnet originates from the breaking Ut and PTt symmetry. As shown in Fig. 2(c), the monolayer Ti_2Se_2S exhibits a semiconductor state with the Hubbard $U = 4.0$ eV under the absence of the SOC effect. The valleys of both valence and conduction bands are degenerate at the X and Y points. Moreover, the VBM at the X point corresponds to spin down band, while the CBM is spin up. Conversely, this spin band is inverted at the Y point. When the SOC is included, as shown in Fig. 2(d), these valleys remain degenerate, since the valley degeneracy is protected by M_{xy} symmetry rather than T symmetry in the magnetic-ferrovalley materials.[50–52] It means that the valley polarization can be only obtained by uniaxial strain, which induces symmetry breaking in the lattice.

It is well known that the on-site correlation Hubbard U value affects the electronic properties of the system. Therefore, we calculate the band structures of Hubbard U in the range of 3.0–4.0 eV. Figure S1 shows the band structures without the SOC effect. When the Hubbard U value is less than 3.1 eV, the monolayer Ti_2Se_2S is the metallic state. The $U = 3.1$ eV is the critical point. As shown in Fig. S1(b), the VBM and CBM just come into contact at the Fermi level. Continuing increasing the Hubbard U value, the X and Y points open a gap and become the semiconductor state. When the SOC is switched on, as shown in Fig. S2, the trend of change is completely consistent without the SOC effect. It is worth noting that the bandgap is opened in E_F-1.5 eV at the Γ point, which may have topological properties. As shown in Fig. S3, the VBM bands are mainly contributed by Ti d_{xy} orbital, while the CBM band is dominated by Ti d_{xz} and d_{yz} orbitals at X and Y points, respectively.

The valleys of monolayer Ti_2Se_2S are protected by mirror M_{xy} symmetry rather than T symmetry. Moreover, the valley polarization does not depend on the SOC effect. If one wants to realize valley polarization in altermagnetic monolayer Ti_2Se_2S, it is necessary to break the M_{xy} symmetry through uniaxial strain. Simultaneously, the rotational symmetry of monolayer Ti_2Se_2S will be lowered from C_4 to C_2. This valley polarization is named piezovalley. Here, the valley splitting of monolayer Ti_2Se_2S is defined as the energy difference ΔV and ΔC between X and Y at the VBM and CBM, $\Delta C(V) = E_{X_{C(V)}} - E_{Y_{C(V)}}$. Therefore, as shown in Figs. 3(a)–3(c) and S4, we investigate the band structure under the uniaxial strain along a direction ranging from −5% to 5% without the SOC effect. At the −4% to 1% uniaxial strain, the VBM remained at the X and Y points. However, the CBM at the Γ point is slightly lower than that at the X and Y points. When the uniaxial tensile strain continues to increase to 2%, the VBM and CBM have transformed into the Γ point. It should be noted that the energy difference between the Γ point and the X/Y points is ∼50 meV. Furthermore, what is even more noteworthy is that they are separated in the momentum space. Therefore, in the following study, our main focus is on the valleys at X and Y points. When the uniaxial compressive strain is applied, the CBM band rises at the X point, and the VBM band drops at the Y point. Consequently, the significant valley polarization produces in the VBM and CBM. The magnitude of the valley polarization is linearly related to the uniaxial strain. Continuously increased to −5% uniaxial compressive strain, the monolayer Ti_2Se_2S turned into a metallic state. While the uniaxial tensile strain is used, the VBM and CBM bands at the Y point will be higher than that at the X point. When the SOC is included, as shown in Figs. 3(d)–3(f) and S5, the band structure is not much different. It is worth noting that the SOC effect has a very minor influence on the valley polarization. Here, we will conduct a comparison by taking −4% uniaxial compressive strain as an example. In the absence of the SOC effect, the valley splittings of valence and conduction bands are 315.06 and 175.58 meV, respectively. When considering the effect of SOC, the valley splittings of valence and conduction bands become 305.28 and 171.68 meV, respectively, compared with the very small effect of valley splitting caused by the lattice symmetry breaking.

In addition, Fig. 4(a) lists the global bandgap variations without and with the SOC effect under the U values ranging from 3.0 to 4.0 eV.

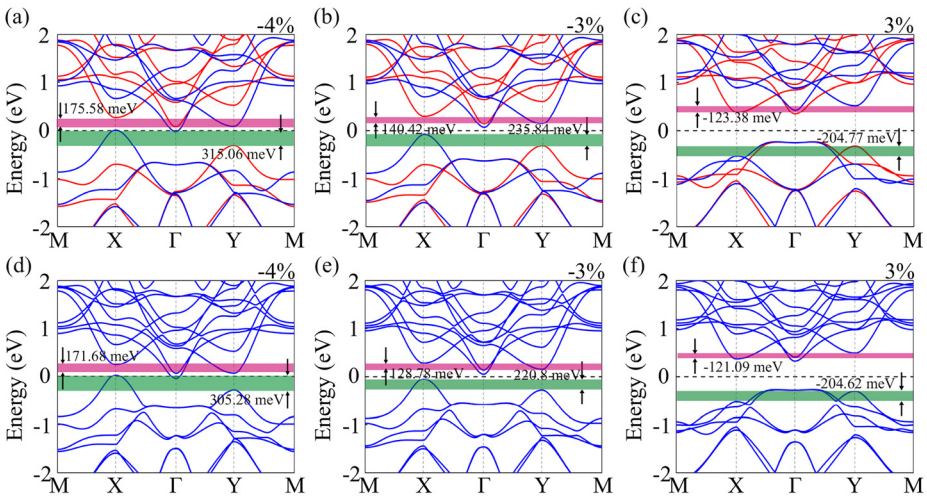

FIG. 3. Spin-polarized band structures of monolayer Ti_2Se_2S with the uniaxial strain, (a) −4%, (b) −3%, and (c) 3%. The red and blue lines denote spin up and spin down bands, respectively. Band structure of monolayer Ti_2Se_2S under the SOC effect with the uniaxial strain, (d) −4%, (e) −3%, and (f) 3%. The valley splitting of valence and conduction bands is exhibited by green and carmine shading, respectively.

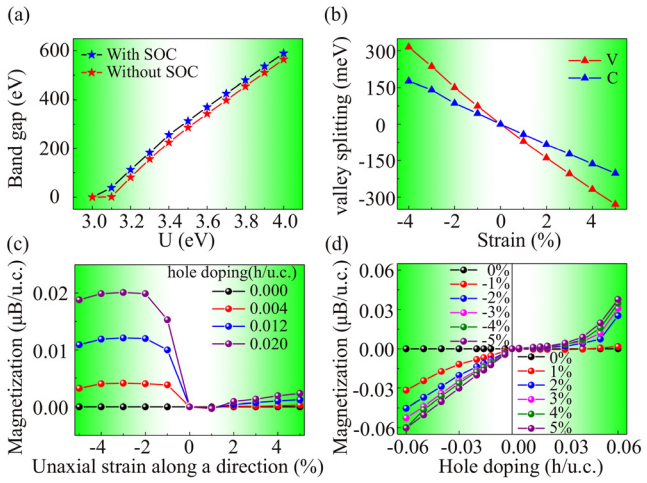

FIG. 4. (a) The global bandgap with and without the SOC effect at the different U values. (b) Valley splitting of monolayer Ti_2Se_2S as a function of uniaxial strain along a direction. The valley splitting of valence and conduction bands is signed the V and C, respectively. (c) The net magnetization per unit cell with the various hole doping amounts under the uniaxial strain along a direction. (d) The net magnetization per unit cell with the various hole doping amounts under the certain uniaxial strain along a direction.

It further indicates that the trend of band structure changes is consistent without and with the SOC effect. The sole difference lies in U = 3.1 eV. The VBM and CBM are in contact with each other at the Fermi level, exhibiting a metallic state without the SOC effect, while it opens the bandgap of 38.30 meV with the SOC effect. In addition, Fig. 4(b) exhibits the valley splitting under the uniaxial strain along a direction. It is clearly demonstrated that the valley splitting can be significantly tuned under uniaxial strain. The adjustable ranges of valence and conduction bands valley splittings are as high as ∼300 and ∼600 meV, respectively. It is far greater than that of monolayer Fe_2Se_2O ∼ 350 meV (valence band),[7] monolayer V_2SeTeO ∼ 300 meV (valence band) and ∼10 meV (conduction band),[53] monolayer Nb_2SeTeO ∼ 50 meV (valence band) and ∼350 meV (conduction band),[54] and so on.

In a magnetic material, the system's magnetism is determined by integrating the spin density over all energies up to the Fermi level. Hence, the net magnetic moment can be induced in the monolayer Ti_2Se_2S by hole or electron doping to shift the Fermi level, such that it crosses only one valley. Based on the symmetry analysis in the aforementioned text, we know that the valley splitting of monolayer Ti_2Se_2S requires a uniaxial strain to break the lattice symmetry. It indicates that the strain-induced valley splitting in the monolayer Ti_2Se_2S affords a method to produce net magnetization. Since the magnetization depends on strain, it is named piezomagnetic property. Currently, the piezomagnetism has been only reported in rare 2D materials, such as V_2Se_2O,[6] Fe_2Se_2O,[7] and V_2SeTeO.[42,53] The net magnetic moment is defined as $M = \int_{-\infty}^{E_f(n)} [\rho^{\uparrow}(\varepsilon) - \rho^{\downarrow}(\varepsilon)]\, dE$, where E_f, n, ε, and $\rho^{\uparrow(\downarrow)}$ are the doped Fermi level, the doping density, external strain, and spin up (spin down) part of the density of states, respectively. As shown in Figs. 4(c) and 4(d), the uniaxial strained monolayer Ti_2Se_2S appears zero net magnetization without doping, since the number of electrons in the occupied states has not changed. The net magnetization exhibits a linear response under the small strain, reaching a saturation value as strain increases. When doped to a certain concentration, the system exhibits strain-dependent magnetization, increasing under uniaxial tension or compressive strains. It is worth noting that the net magnetization of the previously reported V_2Se_2O,[6] Fe_2Se_2O,[7] and V_2SeTeO[42,53] is opposite under the uniaxial compressive and tensile strains. The net magnetization of monolayer Ti_2Se_2S is positive under both uniaxial compressive strain and tensile strain, and the magnetization induced by compressive strain is much larger than that of the tensile strain.

According to the aforementioned calculations and definitions, the valley polarization is zero, positive, and negative values under without strain, uniaxial compressive strain, and uniaxial tensile strain, respectively. Therefore, based on the valley polarization, as shown in Figs. 5(a)–5(c), we defined the logical 0, +1, and −1 states. This implies that the uniaxial strain tunes the valley polarization of monolayer Ti_2Se_2S, and it can be used for signal transmission and storage encoding. In addition, the anomalous valley Hall effect of monolayer

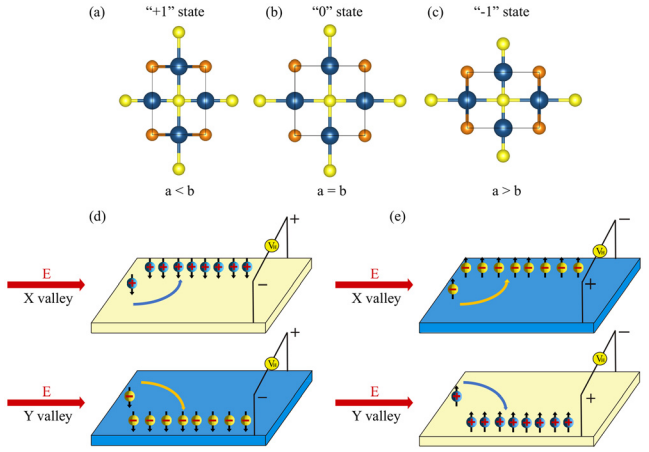

FIG. 5. Top view of the monolayer Ti_2Se_2S crystal structure, (a) uniaxial compressive strain along the a direction, (b) without uniaxial strain, and (c) uniaxial tensile strain along the a direction. Schematic diagram of anomalous valley Hall effect under (d) the uniaxial compressive strain and (e) uniaxial tensile strain at the X and Y valleys. The holes and electrons are represented by the + and – symbols, respectively. Spin up carriers are represented by upward arrows, while spin down carriers are indicated by downward arrows.

Ti_2Se_2S is shown in Figs. 5(d) and 5(e), when the uniaxial compressive strain is applied to monolayer Ti_2Se_2S, as shown in Fig. 5(d). As the Fermi level is tuned to cross between the X and Y points in the VBM band, the spin down holes of X valley will be produced and accumulated on the left edge. When the Fermi level is shifted between the Y and X points in the CBM band, the spin down electrons of Y valley will be generated and accumulated on the right edge. When the compressive strain turns into tensile strain, the situation will be completely reversed. As shown in Fig. 5(e), when the Fermi level once again is moved between the X and Y points in the VBM, the spin up holes of Y valley rather than the spin down holes of X valley will be generated and accumulated on the right edge. Since the uniaxial tensile strain has switched the direction of valley polarization. As the Fermi level is further moved to the region between the X and Y points, the spin up electrons of X valley will be produced and accumulated on the ledge edge. The giant piezovalley effect is anticipated to facilitate multifunction piezovalley application in monolayer Ti_2Se_2S.

In conclusion, based on the DFT calculations, we predict that monolayer Ti_2Se_2S has an out-of-plane altermagnetic ground state and giant valley splitting. The bandgap of altermagnet monolayer Ti_2Se_2S is highly dependent on the Hubbard U value. The monolayer Ti_2Se_2S exhibits a metallic state in the Hubbard $U < 3.1$ eV, while it becomes a semiconductor state in the Hubbard $U > 3.1$ eV. The $U = 3.1$ eV is the critical point, the VBM and CBM bands are in contact at the X and Y points of the Fermi level. By symmetry analysis, we find that the X and Y valleys of altermagnet monolayer Ti_2Se_2S are protected by the mirror M_{xy} symmetry rather than the T symmetry. Therefore, the valley polarization and its switching are achieved via the uniaxial strain along a direction, uncovering a piezovalley phenomenon. The total valley splitting of monolayer Ti_2Se_2S can be as high as ~ 500 meV. In addition, the net magnetization can be induced in the monolayer Ti_2Se_2S doped with holes at the uniaxial strain, showing a piezomagnetic effect. According to the valley polarization, we defined logical 0, +1, and −1 states for data transmission and storage and designed an experimental schematic to detect the anomalous Hall effect. Our work has confirmed that monolayer Ti_2Se_2S is an ideal multipiezo effect candidate material, and the strain engineering offers significant benefits for next-generation multifunctional nanospintronic devices.

See the supplementary material for the additional results.

This work was supported by the National Natural Science Foundation of China (Grants Nos. 12474238 and 12004295). P. Li also acknowledges support from the China's Postdoctoral Science Foundation funded project (Grant No. 2022M722547), the Fundamental Research Funds for the Central Universities (Grant No. xzy012025031), the Open Project of State Key Laboratory of Silicon and Advanced Semiconductor Materials (No. SKL2024-10), and the Open Project of State Key Laboratory of Surface Physics (No. KF2024_02). X. Hu, W. Zhao, and W. Xia thank the National Training Program of Innovation and Entrepreneurship for Undergraduates (Grant No. MSE202410698003).

AUTHOR DECLARATIONS

Conflict of Interest

The authors have no conflicts to disclose.

Author Contributions

Xin Hu, Weihang Zhao, and Wenjun Xia contributed equally to this work.

Xin Hu: Data curation (equal); Formal analysis (equal); Investigation (equal). **Weihang Zhao:** Data curation (equal); Formal analysis (equal); Investigation (equal). **Wenjun Xia:** Data curation (equal); Formal analysis (equal); Investigation (equal). **Hanbo Sun:** Investigation (supporting). **Chao Wu:** Investigation (supporting). **Yinzhong Wu:** Resources (lead). **Ping Li:** Conceptualization (lead); Data curation (equal); Formal analysis (equal); Funding acquisition (lead); Investigation (equal); Methodology (lead); Resources (lead); Software (lead); Supervision (equal); Writing – original draft (lead); Writing – review & editing (lead).

DATA AVAILABILITY

The data that support the findings of this study are available from the corresponding authors upon reasonable request.

REFERENCES

[1]L. Smejkal, J. Sinova, and T. Jungwirth, "Beyond conventional ferromagnetism and antiferromagnetism: A phase with nonrelativistic spin and crystal rotation symmetry," Phys. Rev. X **12**, 031042 (2022).
[2]L. Smejkal, J. Sinova, and T. Jungwirth, "Emerging research landscape of altermagnetism," Phys. Rev. X **12**, 040501 (2022).
[3]Y. P. Zhu, X. Chen, X. R. Liu, Y. Liu, P. Liu, H. Zha, G. Qu, C. Hong, J. Li, Z. Jiang, X. M. Ma, Y. J. Hao, M. Y. Zhu, W. Liu, M. Zeng, S. Jayaram, M. Lenger, J. Ding, S. Mo, K. Tanaka, M. Arita, Z. Liu, M. Ye, D. Shen, J. Wrachtrup, Y. Huang, R. H. He, S. Qiao, Q. Liu, and C. Liu, "Observation of plaid-like spin splitting in a noncoplanar antiferromagnet," Nature **626**, 523 (2024).
[4]J. Krempasky, L. Smejkal, S. W. D'Souza, M. Hajlaoui, G. Springholz, K. Uhlirova, F. Alarab, P. C. Constantinou, V. Strocov, D. Usanov, W. R. Pudelko,

R. G. Hernandez, A. B. Hellenes, Z. Jansa, H. Reichlova, Z. Soban, R. D. G. Betancourt, P. Wadley, J. Sinova, D. Kriegner, J. Minar, J. H. Dil, and T. Jungwirth, "Altermagnetic lifting of Kramers spin degeneracy," Nature **626**, 517 (2024).
[5]M. Naka, S. Hayami, H. Kusunose, Y. Yanagi, Y. Motome, and H. Seo, "Spin current generation in organic antiferromagnets," Nat. Commun. **10**, 4305 (2019).
[6]H. Y. Ma, M. Hu, N. Li, J. Liu, W. Yao, J. F. Jia, and J. Liu, "Multifunctional antiferromagnetic materials with giant piezomagnetism and noncollinear spin current," Nat. Commun. **12**, 2846 (2021).
[7]Y. Wu, L. Deng, X. Yin, J. Tong, F. Tian, and X. Zhang, "Valley-related multipiezo effect and noncollinear spin current in an altermagnet Fe_2Se_2O Monolayer," Nano Lett. **24**, 10534 (2024).
[8]Z. Feng, X. Zhou, L. Smejkal, L. Wu, Z. Zhu, H. Guo, R. G. Hernandez, X. Wang, H. Yan, P. Qin, X. Zhang, H. Wu, H. Chen, Z. Meng, L. Liu, Z. Xia, J. Sinova, T. Jungwirth, and Z. Liu, "An anomalous Hall effect in altermagnetic ruthenium dioxide," Nat. Electron. **5**, 735 (2022).
[9]Q. Cui, B. Zeng, P. Cui, T. Yu, and H. Yang, "Efficient spin Seebeck and spin Nernst effects of magnons in altermagnets," Phys. Rev. B **108**, L180401 (2023).
[10]X. Zhou, W. Feng, R. W. Zhang, L. Smejkal, J. Sinova, Y. Mokrousov, and Y. Yao, "Crystal thermal transport in altermagnetic RuO_2," Phys. Rev. Lett. **132**, 056701 (2024).
[11]H. Reichlova, R. L. Seeger, R. G. Hernandez, I. Kounta, R. Schlitz, D. Kriegner, P. Ritzinger, M. Lammel, M. Leiviska, V. Petricek, P. Dolezal, E. Schmoranzerova, A. Badura, A. Thomas, V. Baltz, L. Michez, J. Sinova, S. T. B. Goennenwein, T. Jungwirth, and L. Smejkal, "Macroscopic time reversal symmetry breaking by staggered spin-momentum interaction," arXiv:2012.15651 (2020).
[12]L. Smejkal, A. B. Hellenes, R. G. Hernandez, J. Sinova, and T. Jungwirth, "Giant and tunneling magnetoresistance in unconventional collinear antiferromagnets with nonrelativistic spin-momentum coupling," Phys. Rev. X **12**, 011028 (2022).
[13]X. Zhou, W. Feng, X. Yang, G. Y. Guo, and Y. Yao, "Crystal chirality magneto-optical effects in collinear antiferromagnets," Phys. Rev. B **104**, 024401 (2021).
[14]Y. Fang, J. Cano, and S. A. A. Ghorashi, "Quantum geometry induced nonlinear transport in altermagnets," Phys. Rev. Lett. **133**, 106701 (2024).
[15]R. G. Hernandez, L. Smejkal, K. Vyborny, Y. Yahagi, J. Sinova, T. Jungwirth, and J. Zelezny, "Efficient electrical spin splitter based on nonrelativistic collinear antiferromagnetism," Phys. Rev. Lett. **126**, 127701 (2021).
[16]S. Karube, T. Tanaka, D. Sugawara, N. Kadoguchi, M. Kohda, and J. Nitta, "Observation of spin-splitter torque in collinear antiferromagnetic RuO_2," Phys. Rev. Lett. **129**, 137201 (2022).
[17]H. Bai, L. Han, X. Y. Feng, Y. J. Zhou, R. X. Su, Q. Wang, L. Y. Liao, W. X. Zhu, X. Z. Chen, F. Pan, X. L. Fan, and C. Song, "Observation of spin splitting torque in a collinear antiferromagnet RuO_2," Phys. Rev. Lett. **128**, 197202 (2022).
[18]S. A. A. Ghorashi, T. L. Hughes, and J. Cano, "Altermagnetic routes to Majorana modes in zero net magnetization," Phys. Rev. Lett. **133**, 106601 (2024).
[19]H. G. Giil and J. Linder, "Superconductor-altermagnet memory functionality without stray fields," Phys. Rev. B **109**, 134511 (2024).
[20]S. Lee, S. Lee, S. Jung, J. Jung, D. Kim, Y. Lee, B. Seok, J. Kim, B. G. Park, L. Smejkal, C. J. Kang, and C. Kim, "Broken Kramers degeneracy in altermagnetic MnTe," Phys. Rev. Lett. **132**, 036702 (2024).
[21]Z. Liu, M. Ozeki, S. Asai, S. Itoh, and T. Masuda, "Chiral split magnon in altermagnetic MnTe," Phys. Rev. Lett. **133**, 156702 (2024).
[22]J. Ding, Z. Jiang, X. Chen, Z. Tao, Z. Liu, T. Li, J. Liu, J. Sun, J. Cheng, J. Liu, Y. Yang, R. Zhang, L. Deng, W. Jing, Y. Huang, Y. Shi, M. Ye, S. Qiao, Y. Wang, Y. Guo, D. Feng, and D. Shen, "Large band splitting in *g*-wave altermagnet CrSb," Phys. Rev. Lett. **133**, 206401 (2024).
[23]M. Zeng, M. Y. Zhu, Y. P. Zhu, X. R. Liu, X. M. Ma, Y. J. Hao, P. Liu, G. Qu, Y. Yang, Z. Jiang, K. Yamagami, M. Arita, X. Zhang, T. H. Shao, Y. Dai, K. Shimada, Z. Liu, M. Ye, Y. Huang, Q. Liu, and C. Liu, "Observation of spin splitting in room-temperature metallic antiferromagnet CrSb," Adv. Sci. **11**, 2406529 (2024).
[24]G. Yang, Z. Li, S. Yang, J. Li, H. Zheng, W. Zhu, Z. Pan, Y. Xu, S. Cao, W. Zhao, A. Jana, J. Zhang, M. Ye, Y. Song, L. H. Hu, L. Yang, J. Fujii, I. Vobornik, M. Shi, H. Yuan, Y. Zhang, Y. Xu, and Y. Liu, "Three-dimensional mapping of the altermagnetic spin splitting in CrSb," Nat. Commun. **16**, 1442 (2025).
[25]I. I. Mazin, K. Koepernik, M. D. Johannes, R. G. Hernandez, and L. Smejkal, "Prediction of unconventional magnetism in doped $FeSb_2$," Proc. Natl. Acad. Sci. **118**, e2108924118 (2021).
[26]Q. Tian, S. I. Vishkayi, M. B. Tagani, L. Zhang, Y. Tian, L. J. Yin, L. Zhang, and Z. Qin, "Two-dimensional artificial Ge superlattice confining in electronic kagome lattice potential valleys," Nano Lett. **23**, 9851 (2023).
[27]R. Wang, M. B. Tagani, S. I. Vishkayi, L. Zhang, L. J. Yin, Y. Tian, Z. Qin, and L. Zhang, "Shape control of few-layer 1T'-WTe_2 flakes via space-restricted chemical vapor deposition," Appl. Phys. Lett. **126**, 171901 (2025).
[28]D. Xiao, W. Yao, and Q. Niu, "Valley-contrasting physics in graphene: Magnetic moment and topological transport," Phys. Rev. Lett. **99**, 236809 (2007).
[29]T. Cao, G. Wang, W. Han, H. Ye, C. Zhu, J. Shi, Q. Niu, P. Tan, E. Wang, B. Liu, and J. Feng, "Valley-selective circular dichroism of monolayer molybdenum disulphide," Nat. Commun. **3**, 887 (2012).
[30]P. Li, B. Liu, S. Chen, W. X. Zhang, and Z. X. Guo, "Progress on two-dimensional ferrovalley materials," Chin. Phys. B **33**, 017505 (2024).
[31]W. Y. Tong, S. J. Gong, X. Wan, and C. G. Duan, "Concepts of ferrovalley material and anomalous valley Hall effect," Nat. Commun. **7**, 13612 (2016).
[32]K. Wang, Y. Li, H. Mei, P. Li, and Z. X. Guo, "Quantum anomalous Hall and valley quantum anomalous Hall effects in two-dimensional d^0 orbital XY monolayers," Phys. Rev. Mater. **6**, 044202 (2022).
[33]P. Li, C. Wu, C. Peng, M. Yang, and W. Xun, "Multifield tunable valley splitting in two-dimensional MXene Cr_2COOH," Phys. Rev. B **108**, 195424 (2023).
[34]P. Li, X. Yang, Q. S. Jiang, Y. Z. Wu, and W. Xun, "Built-in electric field and strain tunable valley-related multiple topological phase transitions in $VSiXN_4$ (X=C, Si, Ge, Sn, Pb) monolayers," Phys. Rev. Mater. **7**, 064002 (2023).
[35]S. D. Guo, L. Zhang, Y. Zhang, P. Li, and G. Wang, "Large spontaneous valley polarization and anomalous valley Hall effect in antiferromagnetic monolayer Fe_2CF_2," Phys. Rev. B **110**, 024416 (2024).
[36]W. Xun, C. Wu, H. Sun, W. Zhang, Y. Z. Wu, and P. Li, "Coexisting magnetism, ferroelectric, and ferrovalley multiferroic in stacking-dependent two-dimensional materials," Nano Lett. **24**, 3541 (2024).
[37]G. Kresse and J. Hafner, "*Ab initio* molecular dynamics for liquid metals," Phys. Rev. B **47**, 558 (1993).
[38]G. Kresse and J. Furthmuller, "Efficient iterative schemes for *ab initio* total-energy calculations using a plane-wave basis set," Phys. Rev. B **54**, 11169 (1996).
[39]G. Kresse and D. Joubert, "From ultrasoft pseudopotentials to the projector augmented-wave method," Phys. Rev. B **59**, 1758 (1999).
[40]J. P. Perdew, K. Burke, and M. Ernzerhof, "Generalized gradient approximation made simple," Phys. Rev. Lett. **77**, 3865 (1996).
[41]S. Grimme, J. Antony, S. Ehrlich, and H. Krieg, "A consistent and accurate *ab initio* parametrization of density functional dispersion correction (DFT-D) for the 94 elements H-Pu," J. Chem. Phys. **132**, 154104 (2010).
[42]W. Xun, X. Liu, Y. Zhang, Y. Z. Wu, and P. Li, "Stacking-, strain-engineering induced altermagnetism, multipiezo effect, and topological state in two-dimensional materials," Appl. Phys. Lett. **126**, 161903 (2025).
[43]B. Goodenough, "Theory of the role of covalence in the perovskite-type manganites [La, *M* (II)]MnO_3," Phys. Rev. **100**, 564 (1955).
[44]J. Kanamori, "Superexchange interaction and symmetry properties of electron orbitals," J. Phys. Chem. Solids **10**, 87 (1959).
[45]P. W. Anderson, "New approach to the theory of superexchange interactions," Phys. Rev. **115**, 2 (1959).
[46]P. Li, X. Li, J. Feng, J. Ni, Z. X. Guo, and H. Xiang, "Origin of zigzag antiferromagnetic orders in XPS_3 (X = Fe, Ni) monolayers," Phys. Rev. B **109**, 214418 (2024).
[47]T. Okugawa, K. Ohno, Y. Noda, and S. Nakamura, "Weakly spin-dependent band structures of antiferromagnetic perovskite $LaMO_3$ (M = Cr, Mn, Fe)," J. Phys.: Condens. Matter **30**, 075502 (2018).
[48]X. Duan, J. Zhang, Z. Zhu, Y. Liu, Z. Zhang, I. Zutic, and T. Zhou, "Antiferroelectric altermagnets: Antiferroelectricity alters magnets," Phys. Rev. Lett. **134**, 106801 (2025).
[49]Z. Zhu, X. Duan, J. Zhang, B. Hao, I. Zutic, and T. Zhou, "Two-dimensional ferroelectric altermagnets: From model to material realization," arXiv:2504.06258 (2025).

[50]Y. Wang, H. Sun, C. Wu, W. Zhang, S. D. Guo, Y. She, and P. Li, "Multifield tunable valley splitting and anomalous valley Hall effect in two-dimensional antiferromagnetic MnBr," Phys. Rev. B **111**, 085432 (2025).
[51]C. Wu, H. Sun, P. Dong, Y. Z. Wu, and P. Li, "Coexisting triferroic and multiple types of valley polarization by structural phase transition in 2D materials," Adv. Funct. Mater. **35**, 2501506 (2025).
[52]H. Sun, Y. Ren, C. Wu, P. Dong, W. Zhang, Y. Z. Wu, and P. Li, "Ferroelectric tuning of the valley polarized metal-semiconductor transition in $Mn_2P_2S_3Se_3/Sc_2CO_2$ van der Waals heterostructures and application to nonlinear Hall effect devices," Phys. Rev. Appl. **23**, 034032 (2025).
[53]Y. Zhu, T. Chen, Y. Li, L. Qiao, X. Ma, C. Liu, T. Hu, H. Gao, and W. Ren, "Multipiezo effect in altermagnetic V_2SeTeO monolayer," Nano Lett. **24**, 472 (2024).
[54]Y. Jiang, X. Zhang, H. Bai, Y. Tian, B. Zhang, W. J. Gong, and X. Kong, "Strain-engineering spin-valley locking effect in altermagnetic monolayer with multipiezo properties," Appl. Phys. Lett. **126**, 053102 (2025).